Mon. Not. R. Astron. Soc. **340,** 1249–1260 (2003)

The relatively young and metal-poor Galactic open cluster NGC 2194

Andrés E. Piatti,[1⋆] Juan J. Clariá[2⋆] and Andrea V. Ahumada[2⋆]

[1] *Instituto de Astronomía y Fisica del Espacio, CC 67, Suc. 28, 1428, Capital Federal, Argentina*
[2] *Observatorio Astronómico, Laprida 854, 5000 Córdoba, Argentina*

Accepted 2002 December 18. Received 2002 December 17; in original form 2002 December 3

ABSTRACT

We present CCD VI_{KC} photometry down to $V \approx 21$ mag in the field of the rich open cluster NGC 2194, which is projected towards the Galactic anticentre direction. We measured V magnitudes and $V - I$ colours for a total of 2515 stars in a field of 13.6×13.6 arcmin^2. These data are supplemented with CCD photometry in the C, M and T_1 filters of the Washington system and photoelectric CMT_1T_2 photometry of 20 red giant candidates. Based on the best fits of isochrones computed by the Geneva and Padova groups to the $(V, V - I)$ colour–magnitude diagram, we derive a colour excess $E(V - I) = 0.75$, a cluster distance of 3.2 kpc and an age of 400 Myr. Five independent Washington abundance indices yield a mean cluster metallicity of [Fe/H] $= -0.27 \pm 0.06$, which is compatible with the existence of both a radial and Z gradient in the Galactic disc. NGC 2194 is a relatively young open cluster, whose deficiency in metal content can be accounted for by the fact that it was born not only far from the Galactic centre in the outer disc, but also at a relatively high Z value.

Key words: techniques: photometric – open clusters and associations: general – open clusters and associations: individual: NGC 2194.

1 INTRODUCTION

Observations reported in this study were carried out as part of a program which has been under way for a number of years at the Observatorio Astronómico de la Universidad Nacional de Córdoba (Argentina). This program undertakes to determine the fundamental parameters or to refine the quality of observationally determined properties of some unstudied or poorly studied open clusters, in order to enlarge our understanding of the clusters themselves and the Galaxy as a whole. Many open clusters with angular diameters exceeding the usual size of the CCD cameras have been studied using *UBV* photoelectric photometry (e.g. Clariá, Lapasset & Bosio 1990; Clariá, Piatti & Lapasset 1998), while many other relatively small angular size open clusters have been investigated using CCD *BVI* Johnson–Cousins photometry (e.g. Piatti, Clariá & Bica 2000; Piatti & Clariá 2001).

NGC 2194 (IAU designation C0611+128), also known as Cr 87 (Collinder 1931), is located in a uniform, moderately rich star field in Orion at $\alpha_{2000} = 6^{\rm h}13\overset{\rm m}{.}8$, $\delta_{2000} = 12^\circ 48'$ and $l = 197\overset{\circ}{.}26$, $b = -2\overset{\circ}{.}33$ (2000). Ruprecht (1966) described it as belonging to Trumpler (1930) class III1r, i.e. a rich, moderately concentrated open cluster with stars in a narrow range of brightness. This object belongs to a group of old and intermediate-age open clusters projected towards the direction of the Galactic anticentre. For research in Galactic structure, the anticentre direction has special interest because in this zone the line of sight intersects the outer arms of the Galaxy without interference from the inner regions. Old distance estimates of NGC 2194 range from 900 to 5010 pc (Alter, Ruprecht & Vanisek 1970), though most recent evidence places it near 3.0 kpc from the Sun. NGC 2194 is in itself worth a detailed study for the number of red giant candidates it contains and the possibility it offers of studying the morphology of the red giant region in connection with previous results (Clariá, Mermilliod & Piatti 1999; Mermilliod et al. 2001; Clariá et al. 2003). Despite this interesting feature recognized in the first cluster photometric study (Cuffey 1943), this object has so far received relatively little attention. del Rio (1980) published colour–magnitude diagrams of NGC 2194 based on photometry of 212 stars in the *RGU* system. He derived a reddening of $E(G - R) = 0.58$, a distance of 2740 pc and an age of 800 Myr. Recently, Sanner et al. (2000) presented much better CCD *BV* data for 2120 stars and a proper motion study in the cluster field. Fitting isochrones to their observed $(V, B - V)$ diagram, they obtained $E(B - V) = 0.45 \pm 0.02$, a distance of 2884 pc and an age of 550 Myr. They were also able to determine the initial mass function of NGC 2194 based on 623 main sequence stars, and found a shallow function with slope of $\Gamma = -1.33 \pm 0.29$. As far as we know, no study of the cluster metal content has yet been made.

We report here the results obtained from CCD VI_{KC} photometry of 2515 stars brighter than $V \approx 21$ mag in the cluster field. These data are supplemented with CCD photometry in the C, M and T_1 filters of the Washington photometric system (Canterna 1976) and photoelectric CMT_1T_2 data of 20 red giant candidates. The advantages

⋆E-mail: andres@iafe.uba.ar (AEP); claria@mail.oac.uncor.edu (JJC); andrea@mail.oac.uncor.edu (AVA)

that the Washington system offers in deriving accurate abundances in yellow and red cluster giants have been clearly pointed out by Geisler, Clariá & Minniti (1991). The VI_{KC} and CMT_1T_2 photometric data are used to derive the cluster fundamental parameters (absorption, distance and age) as well as to estimate the cluster metal content.

In Section 2 we describe the observational material and the data reduction. In Section 3 we present the analysis of the photometric data, while in Section 4 and through the fitting of theoretical isochrones, we determine the cluster parameters reddening, distance, age and metallicity. A brief discussion of the present results is given in Section 5 and a short summary of our conclusions is included in Section 6.

2 OBSERVATIONS AND REDUCTIONS

2.1 CCD *VI* and CMT_1 photometry

CCD images of the cluster field were obtained with the Johnson V, Kron–Cousins I and Washington C, M and T_1 filters, using the 0.9-m telescope at the Cerro Tololo Inter-American Observatory (CTIO), Chile, on 1997 December 23–24. The recommended prescription for the C filter that we used is the one given in Geisler (1996). The telescope was equipped with the 2048 × 2048 pix CCD Tektronix 2K #3 and the seeing was typically 1.5 arcsec during the observing night. The detector used has a pixel size of 24 μm, producing a scale on the chip of 0.4 arcsec pixel^{-1} (focal ratio f/13.5) and a field of view of 13.6 × 13.6 arcmin^2. The CCD was controlled by the CTIO ARCON 3.3 data acquisition system in the standard quad amplifier mode operating at a gain setting of 5 e$^-$/ADU with a readout noise of 4 e$^-$. Note that the standard Washington T_2 filter has long been known to be identical to the Kron-Cousins I filter (Canterna 1976; Bessell 1979). We obtained one 15-s and one 150-s V exposure, one 10-s, one 15-s and one 150-s I exposure, two 50-s C exposures, two 10-s M exposures and three 10-s T_1 exposures for NGC 2194. Fig. 1 shows an schematic finding chart of the observed cluster field.

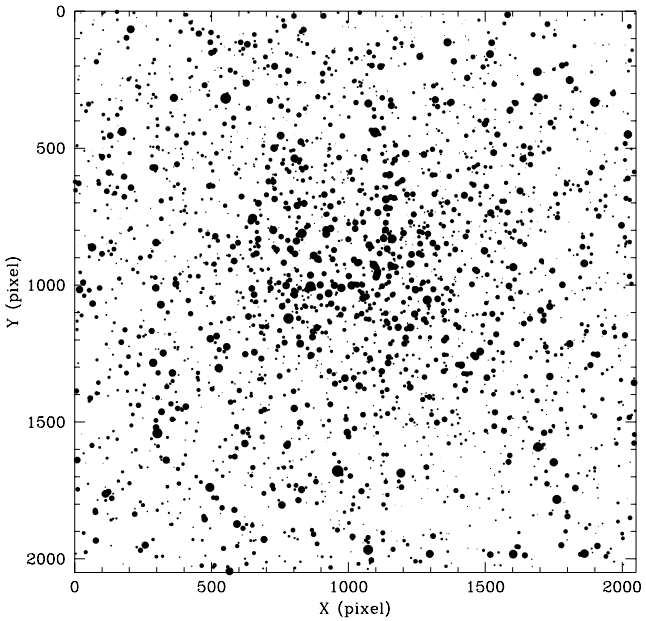

Figure 1. Schematic finding chart of the stars observed in the field of NGC 2194. North is up and east is to the left. The sizes of the plotting symbols are proportional to the V brightness of the star.

The observations were supplemented with a series of 10 bias and five dome and sky flat-field exposures per filter during the observing night to calibrate the CCD instrumental signature. Observations of numerous standard stars from the lists of Landolt (1992) and Geisler (1996) covering a wide range in colour were also observed during the observing night to standardize our photometry.

The VI and CMT_1 images were reduced at CTIO, using QUADPROC tasks of the IRAF software package.[1] The images were bias-subtracted and flat-fielded by employing weighted combined signal–calibrator frames. In addition, we checked for the existence of any illumination pattern on the chip; no correction was necessary. Then, the instrumental magnitudes for the standard and NGC 2194 fields were derived at the Observatorio Astronómico de la Universidad Nacional de Córdoba (Argentina) from aperture photometry and point spread function fits under DAOPHOT/IRAF routines (Stetson 1991), respectively. The relationships between instrumental and standard magnitudes were obtained by fitting the equations

$$v = a_1 + V + a_2X_V + a_3(V - I), \quad (1)$$

$$i = b_1 + V - (V - I) + b_2X_I + b_3(V - I), \quad (2)$$

$$c = c_1 + T_1 + (C - T_1) + c_2X_C + c_3(C - T_1), \quad (3)$$

$$m = d_1 + T_1 + (C - T_1) - (C - M) + d_2X_M + d_3(C - T_1), \quad (4)$$

$$t_1 = e_1 + T_1 + e_2X_{T_1} + e_3(C - T_1), \quad (5)$$

where a_i, b_i, c_i, d_i and e_i (i = 1, 2 and 3) are the coefficients derived through the FITPARAM routine in IRAF, and X represents the effective airmass. Capital and lower-case letters represent standard and instrumental magnitudes, respectively.

Note that for the observing night there are as many instrumental magnitudes per filter as observed standard stars, so that equations (1)–(5) were fitted by least-squares simultaneously. The rms errors affecting the calibration of the equations (1) to (5) are 0.018, 0.006, 0.017, 0.012 and 0.013 mag, respectively. Then, we generated a master table containing a running number, the X and Y coordinates, the V magnitudes and $V - I$ colours, the observational errors $\sigma(V)$ and $\sigma(V - I)$ provided by the IRAF.INVERTFIT task, and the number of observations. This table was built by combining all the independent measurements using the stand-alone DAOMATCH and DAOMASTER programmes kindly provided by Peter Stetson. Table 1 provides this information and is available upon request to the first author of this paper. A portion of this table is shown here for guidance regarding its form and content. In the same way, we built a master table including the T_1 magnitudes and $C - M$, $T_1 - T_2$ and $C - T_1$ colours for all the measured stars, together with the corresponding X and Y coordinates and the photometric errors as deduced from the INVERTFIT task. Note that the Washington $M - T_1$ colours may be derived from the difference between the $C - T_1$ and $C - M$ colours. These photometric data are also available upon request to the first author. Table 2 lists coordinates, T_1 magnitudes, $C - M$, $T_1 - T_2$ and $C - T_1$ colours and the corresponding observational errors

[1] IRAF is distributed by the National Optical Astronomy Observatories, which is operated by the Association of Universities for Research in Astronomy, Inc., under contract with the National Science Foundation.

Table 1. CCD VI data of stars in the field of NGC 2194.

Star	X (pixel)	Y (pixel)	V (mag)	$\sigma(V)$ (mag)	$V-I$ (mag)	$\sigma(V-I)$ (mag)	n
1	154.901	2.301	17.199	0.078	−0.095	0.111	1
2	635.334	3.002	18.836	0.004	1.340	0.109	2
3	108.996	3.036	18.811	0.028	1.329	0.042	1
4	962.257	4.463	18.585	0.044	1.422	0.096	3
5	1041.490	4.493	16.839	0.015	0.889	0.014	3
.	.	.	.	.	.	.	.
.	.	.	.	.	.	.	.
.	.	.	.	.	.	.	.

for only 14 bright and well-isolated red giant candidates located in CCD regions that are free from bad pixels (see Section 4.1).

Fig. 2 shows the trend of the V magnitude and $V-I$ colour errors with V provided by DAOPHOT for NGC 2194. A comparison between our V magnitudes and the CCD V magnitudes determined by Sanner et al. (2000) is shown in Fig. 3. Note that for 1486 stars there is an offset of $\Delta(V_{\rm our}-V_{\rm ccd})=0.04\pm0.06$ mag in common, as well as an indication of some non-linearity in that offset between both magnitude scales.

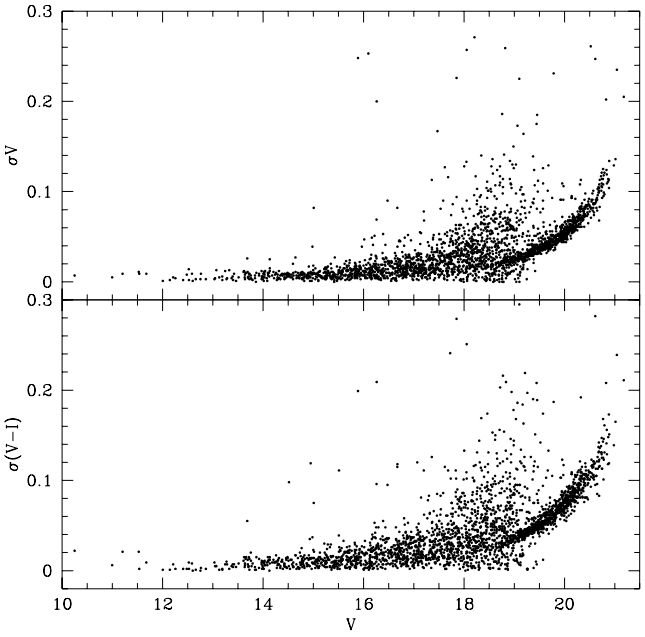

Figure 2. Magnitude and colour photometric errors as a function of V.

2.2 Photoelectric Washington photometry

We also obtained photoelectric photometry with the Washington system C, M, T_1 and T_2 filters for 10 red giant candidates in NGC 2194, during one night in 1993 January with the CTIO 1.0-m telescope. A single-channel pulse-counting photometer was used in conjunction with a dry-ice cooled Hamamatsu R943-02 GaAs photomultiplier. Only one photoelectric measurement was performed for each star. Mean extinction coefficients at CTIO were employed and 17 standard stars from the lists of Canterna & Harris (1979) were used to place the photoelectric observations into the standard Washington system. The colour transformation slopes agree well with those found by Canterna (1976) for CTIO, and the internal mean errors of a single observation are 0.008, 0.009, 0.013 for the $C-M$, $M-T_1$ and T_1-T_2 colours, respectively, and 0.015 for the T_1 magnitudes. These errors are practically independent of the T_1 magnitude. A comparison between the present CCD and photoelectric colours for four stars measured in

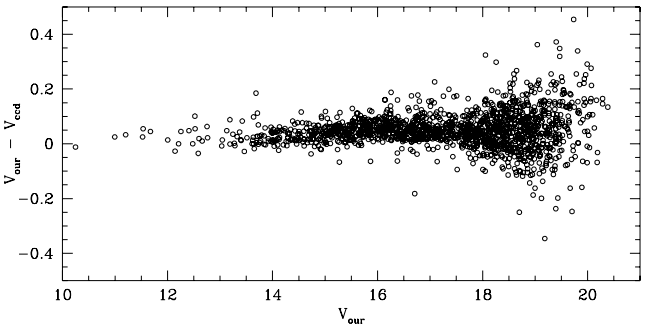

Figure 3. Differences of our $V_{\rm our}$ magnitudes respect to Sanner et al. (2000) $V_{\rm ccd}$ magnitudes as a function of V.

Table 2. CCD Washington photometry of stars in the field of NGC 2194.

Star	X (pixel)	Y (pixel)	$C-M$ (mag)	$\sigma(C-M)$ (mag)	T_1-T_2 (mag)	$\sigma(T_1-T_2)$ (mag)	$C-T_1$ (mag)	$\sigma(C-T_1)$ (mag)	T_1 (mag)	$\sigma(T_1)$ (mag)	n
185	730.28	200.85	1.325	0.006	0.763	0.006	2.405	0.015	13.713	0.008	2
248	627.09	262.30	1.409	0.004	0.811	0.024	2.496	0.031	13.579	0.026	2
303	362.80	316.25	1.806	0.018	0.770	0.019	3.088	0.031	12.638	0.012	2
561	1275.50	522.81	1.325	0.011	0.722	0.037	2.307	0.039	14.134	0.027	2
1064	297.28	844.45	1.285	0.007	0.719	0.011	2.294	0.015	13.274	0.008	2
1187	1861.46	920.67	1.430	0.010	0.748	0.009	2.536	0.012	13.054	0.008	1
1332	296.27	1009.99	1.468	0.005	0.824	0.008	2.635	0.004	13.237	0.010	2
1578	1181.57	1154.10	1.489	0.007	0.821	0.014	2.643	0.004	13.529	0.010	2
1632	495.72	1195.80	1.438	0.005	0.765	0.011	2.578	0.001	13.112	0.004	2
1669	555.56	1224.98	1.576	0.011	0.862	0.004	2.815	0.007	13.197	0.005	2
1698	1481.06	1242.94	1.485	0.010	0.796	0.011	2.618	0.015	12.944	0.011	1
1699	656.53	1245.11	1.762	0.006	0.772	0.021	3.030	0.015	13.763	0.020	2
2422	691.88	1928.99	1.558	0.016	0.822	0.017	2.736	0.023	13.625	0.016	1
2440	257.70	1949.81	1.683	0.016	0.913	0.016	2.925	0.023	13.456	0.015	1

Table 3. Photoelectric CMT_1T_2 data of red giant candidates.

Star	X (pixel)	Y (pixel)	$C-M$ (mag)	$M-T_1$ (mag)	T_1-T_2 (mag)	T_1 (mag)
464	752.603	453.946	1.099	0.889	0.640	13.234
672	1150.776	596.934	1.461	1.092	0.792	13.438
1052	810.176	838.784	1.133	1.015	0.821	13.414
1192	1224.633	922.540	1.315	1.054	0.783	13.268
1379	927.778	1030.212	1.559	1.166	0.822	12.963
1578	1181.575	1154.107	1.515	1.183	0.836	13.590
1632	495.720	1195.809	1.408	1.096	0.801	13.141
1669	555.564	1224.980	1.61	1.210	0.903	13.268
1698	1481.060	1242.942	1.520	1.145	0.809	13.012
1837	987.265	1339.819	1.591	1.231	0.876	13.103

common with both techniques yields $(C-M)_{\rm CCD}-(C-M)_{\rm pe}=-0.017\pm0.026$, $(M-T_1)_{\rm CCD}-(M-T_1)_{\rm pe}=0.008\pm0.028$ and $(T_1-T_2)_{\rm CCD}-(T_1-T_2)_{\rm pe}=-0.026\pm0.012$, thus showing considerable correspondence between the photoelectric and CCD Washington colours. The new photoelectric CMT_1T_2 data for 10 red giant candidates in NGC 2194 are presented in Table 3.

3 ANALYSIS OF THE DATA

Fig. 4 shows the resulting $(V, V-I)$ colour–magnitude diagram (CMD) obtained using all the measured stars. A first glance at the figure reveals a crowded broad sequence of stars which traces the cluster main sequence (MS), and a prominent clump of red stars at $(V, V-I)\sim(14, 1.6)$. The precise definition along 7 mag of the MS lower envelope is absolutely remarkable, in contrast to the blurry appearance of the MS upper envelope which suggests the possible existence of field contamination, differential reddening and/or intrinsic dispersion (e.g. binarity, evolutionary effects), or else a combination of all these effects. Another interesting feature of the $(V, V-I)$ CMD is the presence of a number of good candidates for blue stragglers (BSs). There are 22 stars above the turn-off and bluer

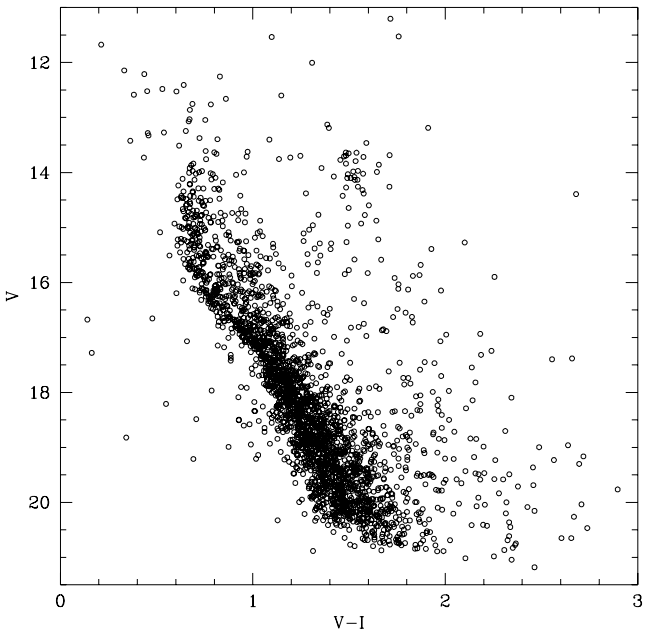

Figure 4. $(V, V-I)$ colour–magnitude diagram for stars observed in the field of NGC 2194.

than $V-I=0.8$ in the area where BS stars are commonly found. Of these, 17 are within 5 arcmin of the cluster centre. Although without knowing the radial velocities we cannot assess membership of these stars, based on statistical grounds we may reasonably expect many of them to be cluster members. Note that star #1207 of our sample, equivalent to del Rio #160 or Sanner et al. (2000) #38, is the only one considered to be a BS in the catalogue of blue stragglers in open clusters of Ahumada & Lapasset (1995).

A simple inspection of the photometric data shows that 49 per cent of the total number of measured stars have three measures of their V magnitudes and $V-I$ colours and approximately expand from =13 down to 19, while 16 and 35 per cent of the measured stars have two and one measures and cover V ranges of 15–19.5 and 18.5–21 mag, respectively. Thus, stars with three measures that also have small photometric errors become a valuable reference to the reliability of the morphology and position of the main cluster features. These cluster features apparently remain unaltered when Fig. 4 is constructed using only stars with photometric uncertainties within 0.01 mag from the mean error at any V magnitude level. This result might seem to indicate that the broadness and scatter of the cluster MS is not originated by errors in our photometry. In the subsequent analysis we refer to as the broadness of the MS to the upper MS, as for the very lower MS, the broadness is mainly due to the errors in $V-I$.

With the aim of exploring the origin of the observed scatter towards the redder end of the cluster MS, we decided to get hold of proper motions determined by Sanner et al. (2000). However, as only a handful of bright stars have probabilities of being cluster members higher than 80 per cent – the limiting membership criterion adopted by them – in common with Sanner et al., we did not find such information helpful for our purposes. All these stars proved to be brighter than $V=15$ as is similarly shown in their fig. 14.

The contamination by field stars can also disturb the drawing of a clearer outline of the right-hand side of the cluster MS. As we did not take any comparison field around the cluster, we evaluated such a possibility in the cluster CMD by first determining the cluster centre, and then constructing its stellar density profile from which we estimated the cluster radius. To determine the central coordinates of the cluster we simply used the finding chart of Fig. 1 instead of a statistical approach. The relatively high space resolution of the images obtained and the presence of groups of stars spreading out throughout the field, produced spurious peaks in the projected X and Y stellar distribution which mimic central cluster regions, assumed to be those of the highest stellar densities. Therefore, we adopted as the cluster centre the position $(X_C, Y_C)=(1000, 1010)$ pixel by looking at Fig. 1. We then traced the cluster stellar density profile from the count of the number of stars per pixel in rings of 30 pixel wide centred on the cluster. No more detailed stellar profile is provided using a narrower ring size, but additional noise which increases as the radial interval gets smaller. Fig. 5 presents the resulting stellar density distribution, which shows that cluster stars are distributed within an area with a radius of $\sim$800 pixel from the cluster centre, most of them lying inside $\sim$360 pixel. The horizontal line in Fig. 5 indicates the estimated background level. Therefore, we adopted 800 pixel, equivalent to 5.3 arcmin, as the cluster radius. The fact that NGC 2194 appears to cover most of the CCD field prevents us from attributing the MS broadness to the contamination of field stars surrounding the cluster, although field stars were certainly observed along its line of sight.

We looked into the nature of the broadness of the cluster MS following a different approach, which consists in examining the distribution in the cluster field of stars placed at different distances

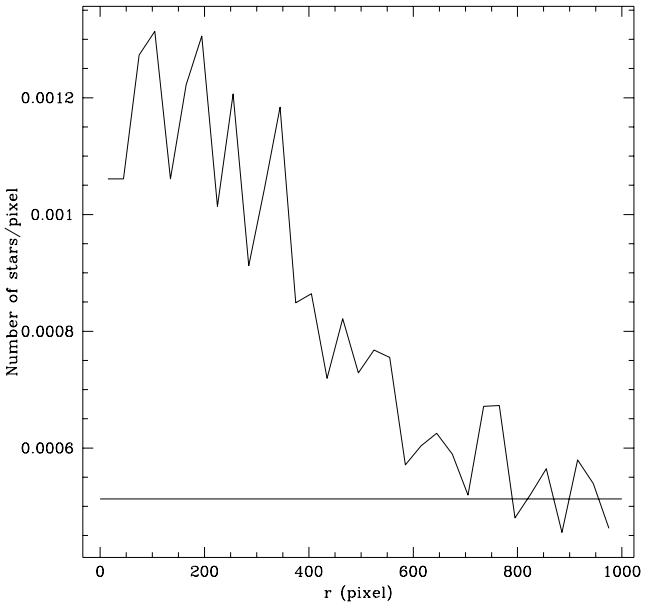

Figure 5. Stellar density profile centred at $(X_C, Y_C) = (1000, 1010)$ pixel for stars observed in the field of NGC 2194.

from the fiducial cluster MS. First, we defined the fiducial cluster MS as the curve joining the points on the cluster MS with the highest star densities. Fig. 6 shows the resulting fiducial sequence by means of a thick solid line. Secondly, in order to take into account the photometric errors, we fitted $\sigma(V)$ and $\sigma(V-I)$ in terms of V (Fig. 2) using the CURFIT task executable within the IRAF environment. Mean $\sigma(V)$ and $\sigma(V-I)$ points at different V magnitudes were adjusted using Legendre functions of the order of 6 for $V \geqslant$ 17 mag, and assumed to be equal to 0.01 mag for $V < 17$. Then, we defined the cluster MS width due to photometric errors as the distance at any V magnitude level between points which are separated by $3\sigma(V-I)$ from the fiducial cluster MS. Thin solid lines in Fig. 6 at both sides of the fiducial cluster MS represent the lower and upper limits of the defined MS width. Notice that lacking any other source for colour dispersion, cluster MS stars should be inside this zone. Otherwise, cluster stars with redder $V-I$ colours could be affected by differential reddening or evolutionary effects. Thirdly, we shifted redwards the fiducial cluster MS until we reached the lower limit estimated by Burki (1975) for clusters with differential reddening, $\Delta(B-V) = 0.11$, which corresponds to $\Delta(V-I) = 0.15$ if a value of 1.33 for the $E(V-I)/E(B-V)$ ratio (Cousins 1978) is adopted. This curve is drawn in Fig. 6 with short dashed lines. Finally, we also traced the fiducial cluster MS with an offset twice that of the Burki's value (dotted line), i.e. $\Delta(V-I) = 0.30$, for the sake of comparison.

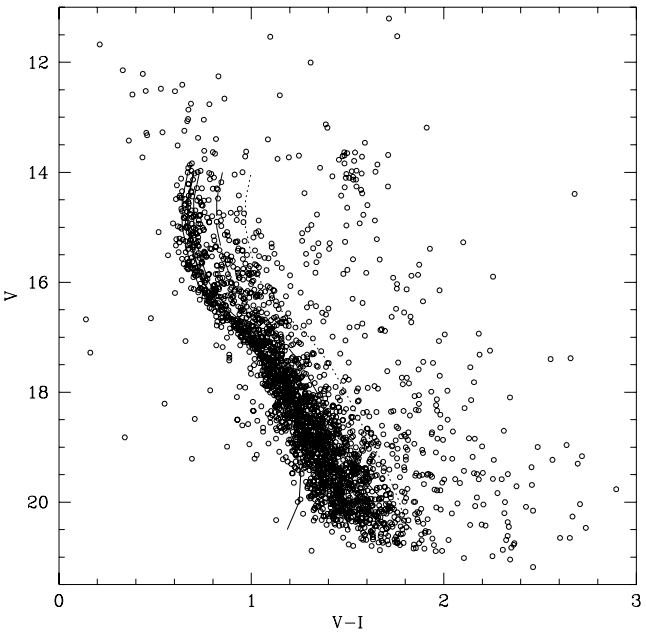

Figure 6. $(V, V-I)$ colour–magnitude diagram for stars observed in the field of NGC 2194. The fiducial cluster Main Sequence (MS), the $\pm 3\sigma(V-I)$ shifted MS, the Burki's limit shifted MS and the $\Delta(V-I) = 0.30$ shifted MS are also drawn with thick solid, thin solid, short dashed and dotted lines, respectively (see details in Section 3).

Fig. 7 depicts the distribution of stars in the observed field which are placed in different slices along the cluster MS as illustrated in Fig. 6, namely inside the cluster MS width (upper left-hand panel), between the upper limit of this region and the Burki's limit (upper right-hand panel), from the Burki's limit as far as $\Delta(V-I) = 0.30$ (lower left-hand panel), and beyond this shifted MS (lower right-hand panel). As can be seen, most of the observed stars lie within the photometric limits defined from the fiducial cluster MS and the $V-I$ errors of Fig. 2. Stars in the upper right-hand panel are notably concentrated within a region which agrees well with the estimated full width at half maximum (FWHM) of the stellar density profile of Fig. 5, while stars with $V-I$ colours redder than those for the Burki's limit and bluer than the $\Delta(V-I) = 0.30$ shifted MS (lower left-hand panel) appear to be distributed more uniformly throughout the field. If these latter stars were cluster members, we could draw the conclusion that NGC 2194 is affected by some amount of differential reddening. However, because stars from the lower right-hand panel of Fig. 7 also show a similar relatively uniform star distribution, we favour the possibility that an important percentage of the stars in the lower left-hand panel are field stars instead of considering them as cluster stars affected by differential reddening. Thus, we conclude that the broadness of the NGC 2194 MS is mainly caused by intrinsic features such as binarity and/or evolutionary effects, although a small but non-negligible number of field stars located along the line of sight of the cluster are also present.

4 CLUSTER FUNDAMENTAL PARAMETERS

The widely used procedure of fitting theoretical isochrones to the observed CMD was employed to estimate the $E(V-I)$ colour excess, the $V - M_V$ apparent distance modulus, the age and the metallicity of NGC 2194. We took advantage of the extended and clearly shaped cluster MS, as well as of the presence of a conspicuous cluster giant clump (GC). Two sets of theoretical models were taken into account. On the one hand, we used the isochrones calculated by Lejeune & Schaerer (2001, hereafter LS01) for the entire set of non-rotating Geneva stellar evolution models, covering masses from 0.4–0.8 to 120–150 $M_\odot$ and metallicities from $Z = 0.0004$ to 0.1. The isochrones expand the age range from 10^3 yr to 16–20 Gyr in steps of $\Delta \log t = 0.05$ dex. On the other hand, we used tables of theoretical isochrones built by Girardi et al. (2002) on the basis of a re-written formalism for converting several sets of Padova isochrones into absolute magnitudes and colours of

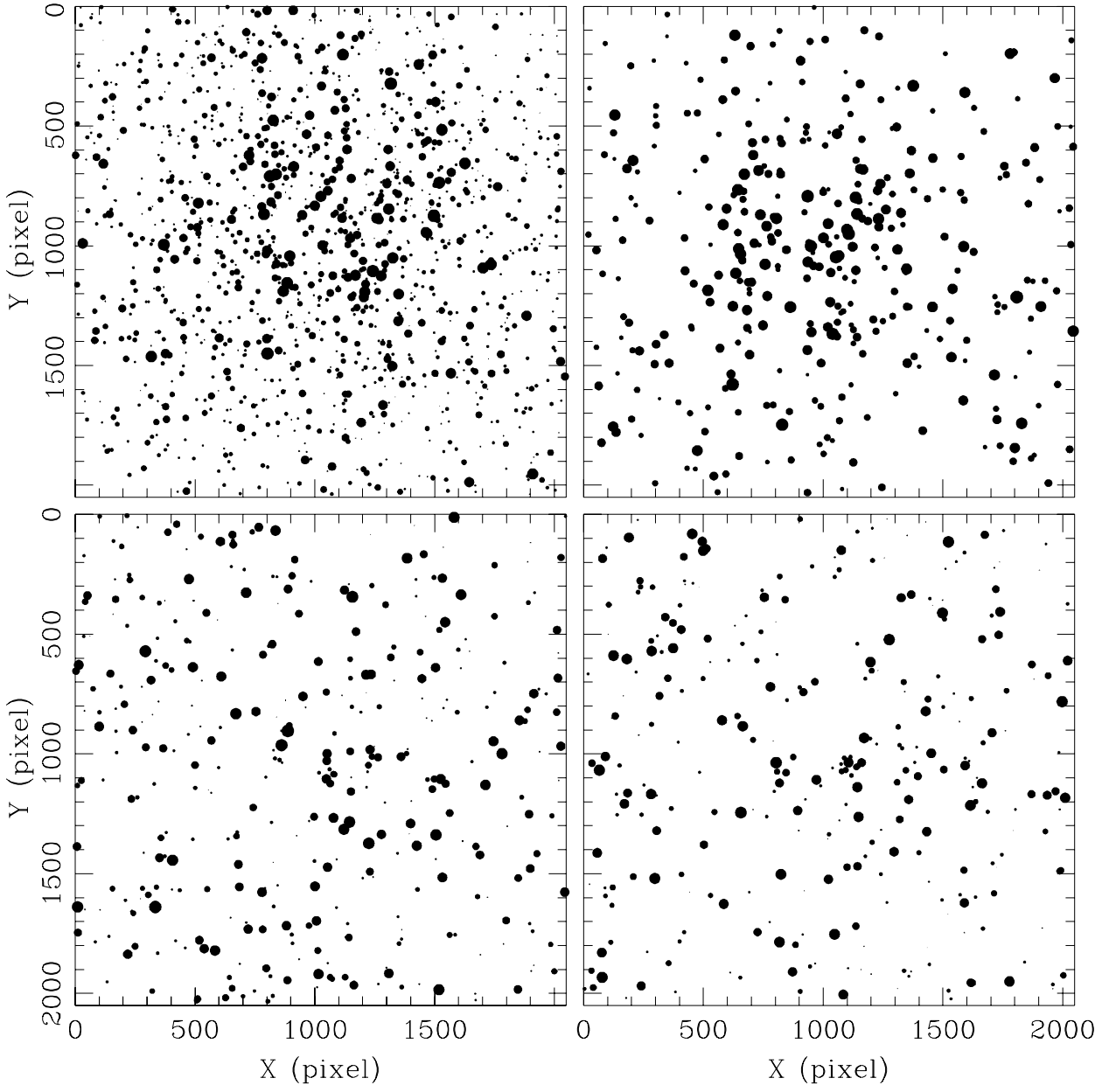

Figure 7. Schematic finding charts of the stars distributed inside the $\pm 3\sigma(V-I)$ shifted MS (upper left-hand panel), between $+3\sigma(V-I)$ and Burki's limit MSs (upper right-hand panel), from Burki's limit until $\Delta(V-I)=0.30$ shifted MS (lower left-hand panel), and beyond $\Delta(V-I)=0.30$ shifted MS (lower right-hand panel).

different photometric systems. Bolometric corrections are obtained from the resulting formulae and synthetic stellar spectra, provided that the zero-points are specified by means of well-known spectrophotometric standards.

Concerning the fit, we used the brightness of both the GC and the MS turn-off (TO) and the $V-I$ colour of the TO, as references for selecting a subsample of isochrones computed by the Geneva and Padova groups, respectively, including the overshooting effect. In order to address the metallicity effect in the cluster fundamental parameters, subsets of isochrones for different Z values were selected. The best simultaneous match to the cluster MS and GC is achieved by the isochrone of $\log t = 8.6$ and $Z = 0.008$. From this fit we derive $E(V-I) = 0.75$ and $V - M_V = 14.25$ mag. The uncertainty in the choice of the most resembled isochrone to the cluster MS and GC due to a random combination of age and metallicity is 50 Myr, which in turn translates into errors in $E(V-I)$ and $V - M_V$ of 0.05 and 0.25 mag, respectively. Once the above reddening and distance modulus are adopted, the combination of varying age and metal abundance in the fitting procedure of LS01 isochrones is illustrated in Fig. 8, where four different isochrones were superimposed to the cluster CMD for three distinct metallicities. For the sake of completeness we also show in Fig. 9 the results of the fitting by using the Girardi et al. (2002) isochrones. Notice that the cluster MS is satisfactorily fitted within the errors by the isochrone corresponding to $\log t = 8.6$ of LS01, and that of Girardi et al. (2002) as well. The isochrones also appear to tightly fit possible cluster stars placed in the transition path from the MS to the GC. By using the derived $E(V-I)$ reddening and apparent distance modulus and

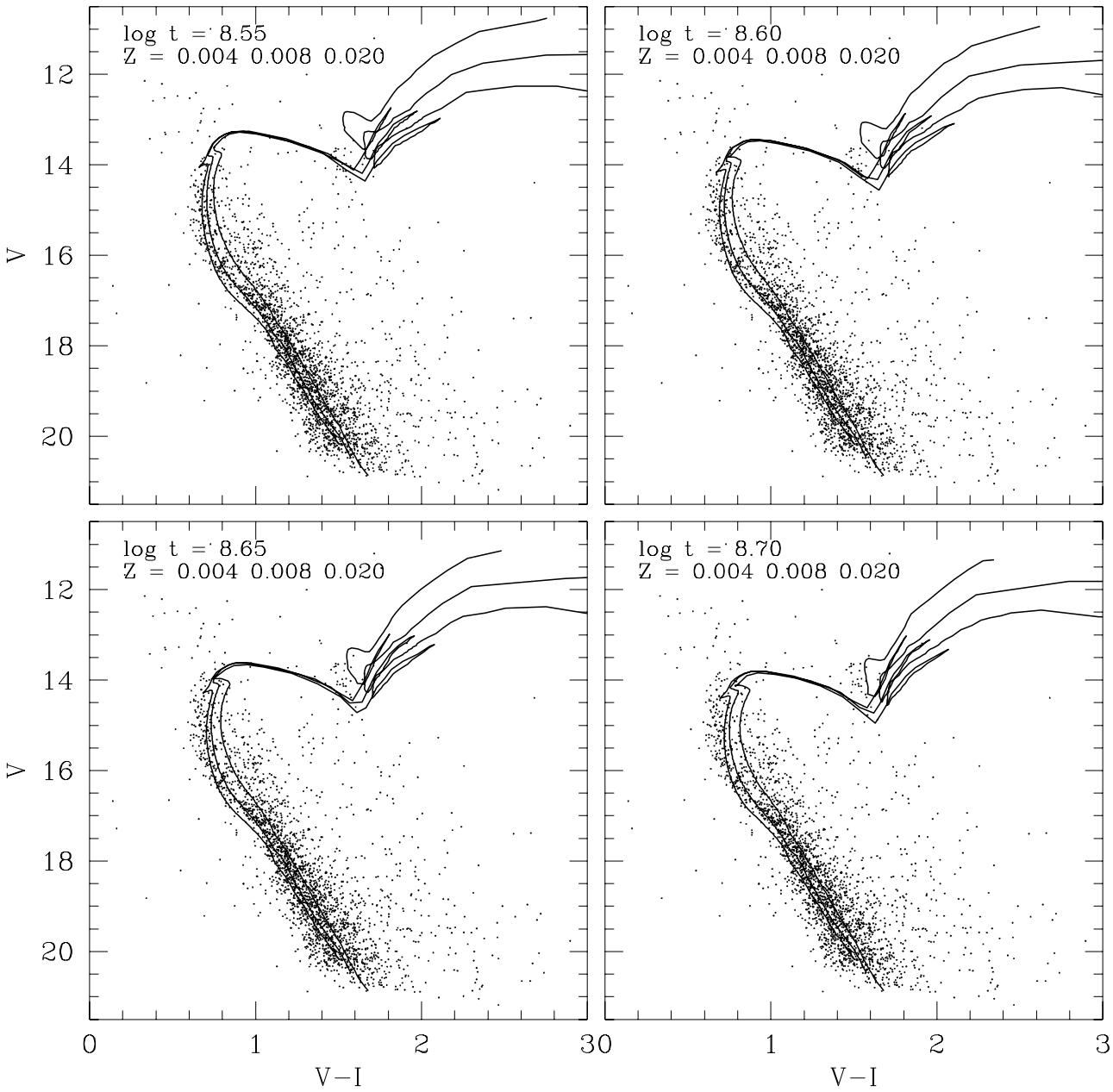

Figure 8. $(V, V-I)$ CMDs for NGC 2194 stars. Isochrones from Lejeune & Schaerer (2001), computed taking into account overshooting, are overplotted.

the most frequently used values for the $E(V-I)/E(B-V)$ and $A_V/E(B-V)$ ratios (Cousins 1978), we obtained $E(B-V) = 0.55 \pm 0.05$ and $V_o - M_V = 12.5 \pm 0.5$, which implies a distance from the Sun of 3.2 ± 0.6 kpc. The distance error was computed with the expression: $\sigma(d) = 0.46\{\sigma(V-M_V) + 3.2\,\sigma[E(B-V)]\}d$, where $\sigma(V-M_V)$ and $\sigma[E(B-V)]$ represent the estimated errors in $V-M_V$ and $E(B-V)$, respectively. Note that the $E(B-V)$ reddening value turned out to be considerably greater than the value derived by Sanner et al. (2000).

Fig. 10 shows an enlargement of the GC region. Isochrones corresponding to $\log t = 8.6$ and $Z = 0.008$ calculated by both groups have been superimposed in this figure. The loop corresponding to the bluest stage during the He-burning core phase in both isochrones is shifted towards redder colours with respect to the position of the cluster GC, approximately $\Delta(V-I) = 0.15$–0.20 mag, the LS01 loop being slightly bluer. Theoretical GCs have also frequently proved to be redder than the observed GCs in previous studies of star cluster spanning ages from 0.3 up to 2.3 Gyr (Meynet, Mermilliod & Maeder 1993; Clariá et al. 1994; Rosvick 1995; Geisler et al. 2003), although some other studies have found excellent agreement between theory and observations for red clumps of intermediate age clusters (Mermilliod et al. 2001). Particularly, Piatti, Clariá & Bica (1998) confirmed the existence of a shift between the observed loops and the theoretical ones for clusters older than 200 Myr from the comparison of empirical and Padova isochrones. Using their empirical isochrones, we obtained $E(V-I) = 0.70 \pm 0.05$, $V - M_V = 14.25 \pm 0.50$ and an age of 300 ± 50 Myr for NGC 2194, in good agreement with the adopted cluster parameters. The cluster GC falls inbetween those of the template clusters NGC 6259 (age = 200 Myr) and NGC 3680 (age = 2.0 Gyr).

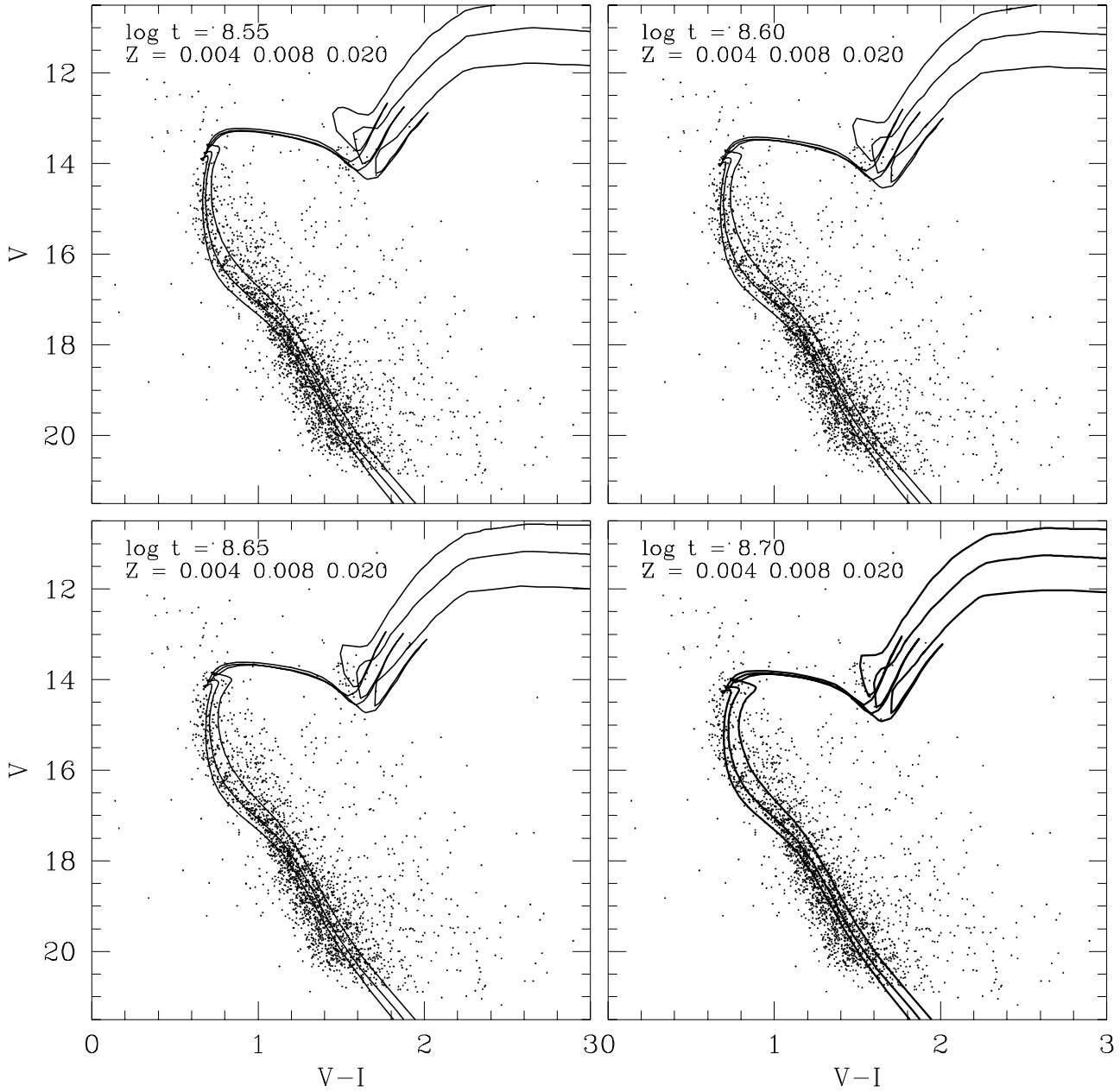

Figure 9. $(V, V-I)$ CMDs for NGC 2194 stars. Isochrones from Girardi et al. (2002), computed taking into account overshooting, are overplotted.

4.1 Metal content

Geisler, Clariá & Minniti (1991, hereafter GCM91) have calibrated five Washington metallicity sensitive indices in terms of high dispersion spectroscopic iron-to-hydrogen ratios and proposed an iterative method to estimate metal abundances of late-type giants. The method allows for mean cluster abundances to be easily obtained after a few iterations, although the accuracy of the resulting metallicity values strictly depends on the quality of the photometric data. As far as we are aware, only photoelectric Washington colour indices with a precision of the order of ∼0.01 mag have been used up to now (e.g. Clariá, Mermilliod & Piatti 1999; Mermilliod et al. 2001), and no CCD CMT_1T2 photometric study has yet reported mean open cluster metallicities. Wee & Lee (1996) and Wee, Lee & Geilser (1996) obtained only very preliminary [Fe/H] values for the open clusters NGC 1245 and Tombaugh 2 using CCD Washington data, but no explanation about the uncertainties involved in the adopted abundances are given. Therefore, for the stars observed with the CCD technique in NGC 2194, we conservatively keep those stars that verify $m_f(i = 14) - m_f(i = 15) < 0.01$ mag, where $m_f(i)$ is the instrumental magnitude of a star measured through the passband f with aperture of i pixels in radius. This criterion constrains the selection of stars to those bright and well isolated stellar objects placed in free-bad pixel CCD regions. Table 2 lists coordinates, colours and magnitudes of 14 stars which satisfy the established requirement.

GCM91 defined fiducial lines for solar-abundance giants in the Washington system colour–colour (CC) diagrams, including the $(C-T_1)_o/(T_1-T_2)_o$, $(C-M)_o/(M-T_2)_o$ and $(C-T_1)_o/(M-T_2)_o$ relations. They defined the abundance-sensitive index Δ as the difference between the observed colour and the solar-abundance colour at the observed $(T_1-T_2)_o$ [or $(M-T_2)_o$], where all colours

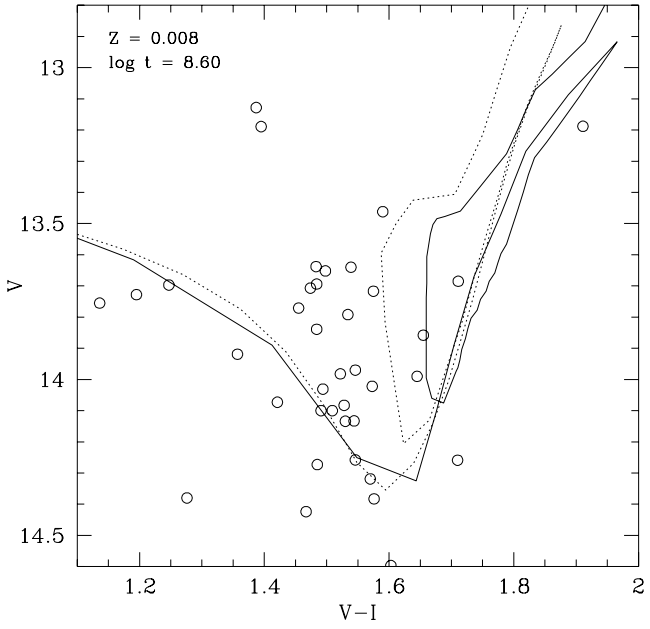

Figure 10. $(V, V-I)$ CMDs for stars in the red clump region of NGC 2194. The isochrone for $\log t = 8.6$ and $Z = 0.008$ from Girardi et al. (2002) and Lejeune & Schaerer (2001) is overplotted with solid and dotted lines, respectively.

refer to dereddened values. For example, $\Delta_1 = \Delta(C-M)_{T_1-T_2} = (C-M)_o - (C-M)_s$, where $(C-M)_o$ is the observed $C-M$ value corrected for reddening and $(C-M)_s$ is the solar abundance $C-M$ for a star with the observed (reddening-corrected) $(T_1 - T_2)_o$.

GCM91 also demonstrated that the calibration of the Washington abundance indices is affected by systematic errors due to the decrease of abundance sensitivity with temperature and established empirical calibrations of five abundance indices $\Delta'_1 - \Delta'_5$ with [Fe/H], where $\Delta'_1 - \Delta'_5$ refer respectively to $\Delta'(C-M)_{T_1-T_2}$, $\Delta'(M-T_1)_{T_1-T_2}$, $\Delta'(C-T_1)_{T_1-T_2}$, $\Delta'(C-M)_{M-T_2}$ and $\Delta'(C-T_1)_{M-T_2}$. These indices can be calculated from the Δ indices as described by GCM91 using their equation (2). In particular, $\Delta' = \Delta$ for stars with $(T_1 - T_2)_o = 0.57$ or $(M-T_2)_o = 1.45$.

To determine the cluster metal content we have used the photometric information of 20 red giant candidates (Tables 2 and 3), obtained from the blue and green spectral regions. This is due to the fact that for G and K stars, the abundance parameters based on these spectral regions are sensitive to metallic line blanketing (primarily due to iron) and to metallic plus molecular (CN and CH) absorption. As mentioned in Section 2.2, four stars were observed in common with the CCD and photoelectric techniques so that their unweighted averaged colours have been adopted. For each star we determined the five metallicity indices $\Delta'_1 - \Delta'_5$, using the adopted cluster value $E(B-V) = 0.55$ and the reddening ratios given by GCM91. Stars #185, 464, 561, 1064 and 1187 were omitted because they fall outside the range of the empirical calibrations. Fig. 11 displays the five unreddened Washington CC diagrams for the remaining red giant candidates. Iso-abundance lines for [Fe/H] $= +0.5$, 0.0, -0.5 and -1.0 are shown in this figure, except for the $(M-T_1)_o/(T_1-T_2)_o$ diagram wherein iso-abundance lines corresponding to [Fe/H] $= +0.4, 0.0, -0.4$ and -0.8 are plotted. Note that six stars (#303, 1052, 1669, 1699, 1837 and 2440) appear to be significantly more metal-poor or more metal-rich than the cluster giants so that these stars, represented by open circles in Fig. 11, have not been considered in the metallicity determination. The five Washington abundance indices Δ' derived for the remaining nine stars are given in Table 4. The resulting mean values and corresponding standard deviations are: $\Delta'_1 = -0.114 \pm 0.032$, $\Delta'_2 = -0.021 \pm 0.019$, $\Delta'_3 = -0.140 \pm 0.052$, $\Delta'_4 = -0.082 \pm 0.032$ and $\Delta'_5 = -0.087 \pm 0.035$, which in turn imply [Fe/H]$_1 = -0.28 \pm 0.09$, [Fe/H]$_2 = -0.20 \pm 0.13$, [Fe/H]$_3 = -0.28 \pm 0.13$, [Fe/H]$_4 = -0.30 \pm 0.13$ and [Fe/H]$_5 = -0.27 \pm 0.11$, if the calibrations of GCM91 are used. The difference between the abundances derived from the iron lines and those obtained from the blue spectral features contaminated by CN and CH is not overly significant, considering the photometric and calibration errors. This fact leads us to conclude that the cluster giants are not enriched in elements of the CNO group. The unweighted mean of the five abundance estimates, i.e. [Fe/H] $= -0.27 \pm 0.03$, has been adopted for NGC 2194. The metallicity error corresponds to the standard deviation of the five independent [Fe/H] values derived from the Δ' indices. The resulting Washington metallicity for NGC 2194 is in very good agreement with that inferred from the isochrone fitting procedure.

5 DISCUSSION

The resulting cluster reddening and distance estimates place NGC 2194 among the relatively most reddened and distant studied open clusters located towards the cluster direction, a result which is illustrated in Fig. 12. With the help of the WEBDA Open Cluster Data Base (see, http://obswww.unige.ch/webda/), we selected a list of clusters distributed within a region of $15^\circ \times 15^\circ$ centred on NGC 2194, defined by $190^\circ \leqslant l \leqslant 205^\circ$ and $-10^\circ \leqslant b \leqslant 5^\circ$, and with known values of their colour excesses, distances and ages. In Table 5 we present the final cluster list with the values of the adopted parameters and corresponding references, having averaged the involved quantities when two or more references were used. Open circles represent these clusters, while a star identifies NGC 2194. The upper left-hand panel shows the cluster angular distribution, which reveals a remarkable tendency of the clusters to be located close or in the Galactic plane. This characteristic is also visible in the upper right-hand panel of Fig. 12. On the other hand, the $E(B-V)$ versus d relationship shows the commonly expected simple result that, the farther the cluster is located along the same line of sight, the higher the interstellar reddening estimate, because of the increase of the dust column with the cluster distance. This result has no quarrel with the existence of more or less reddened open clusters, which is rather a consequence of the non-uniform distribution of the dust with the Galactic coordinates.

Both right-hand panels of Fig. 12 show that three clusters (NGC 2141, Berkeley 22 and Trumpler 5) are older, and two of them (NGC 2141 and Berkeley 22) are farther out the Galactic plane than NGC 2194. The three older clusters ($2.5 \leqslant$ age $\leqslant 4.1$ Gyr) have probably travelled through the Galactic disc, crossing the Galactic plane several times (Carraro & Chiosi 1994; Piatti, Clariá & Abadi 1995), and are presently observed at different heights (Z). In addition, they have been born at higher $|Z|$ values than the younger ones, becuase if they had been born near the Galactic plane they might have had initial perpendicular velocities in order to reach higher $|Z|$ values, which is unlikely for objects with birthplaces confined to low $|Z|$ values. Notably, NGC 2194, although more than 6 times younger than these 2–4 Gyr old clusters, has also been born at a higher $|Z|$ value (its present $|Z|$ value is 0.13 kpc) than coeval or younger clusters.

According to the generally accepted image of a radial abundance gradient for the Galactic disc, one would expect NGC 2194 to be

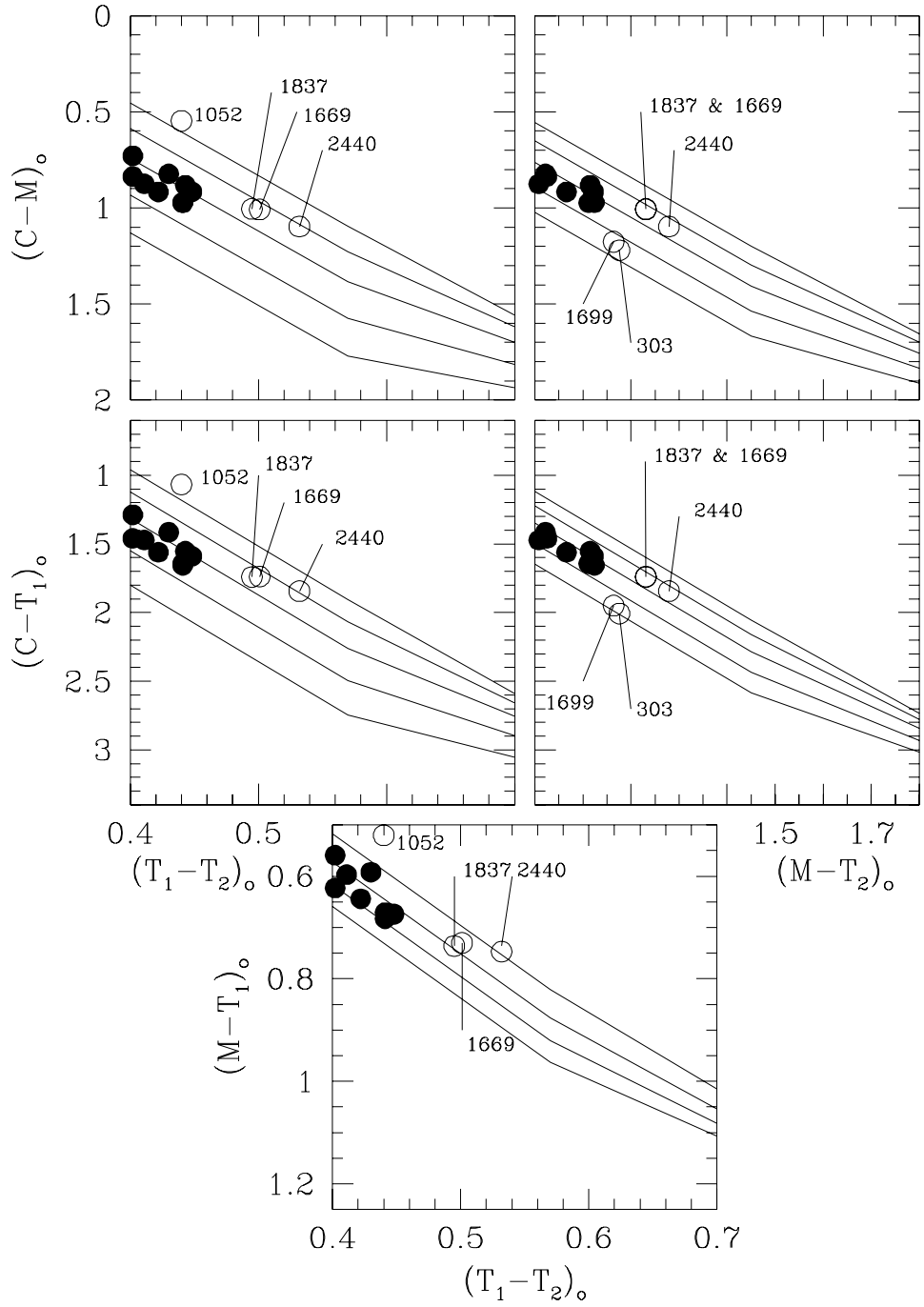

Figure 11. Red giant candidates observed in the Washington system plotted in the different unreddened two-colour diagrams from which the Δ'_i abundance parameters are derived. Iso-abundance relations from GCM91 for 0.5 dex intervals from [Fe/H] $= -1.5$ to 0.5 are shown, except for the $(M - T_1)_o$ /$(T_1 - T_2)_o$ diagram wherein iso-abundance relations for 0.4 dex intervals from [Fe/H] $= -0.8$ to $+0.4$ are given. Stars considered to be probable red cluster giants are represented with filled circles, while those significantly more metal-poor or metal-rich than the cluster giants are represented with open circles.

-0.22 ± 0.03 dex more metal-poor than the Sun, if a value of ∂[Fe/H]$/\partial R_{\rm GC} = -0.07 \pm 0.01$ dex kpc^{-1} is adopted for the radial abundance gradient (Piatti, Clariá & Abadi 1995; Rolleston et al. 2000). This is the metallicity corresponding to an object located in the Galactic plane ($Z = 0.0$) and 3.2 kpc farther from the Sun toward the Galactic anticentre. However, NGC 2194 is even more metal-poor than this radial gradient based metallicity value. This small metallicity difference could be explained in terms of a perpendicular abundance gradient, for which farther objects are more metal-poor. Piatti et al. (1995) derived a perpendicular abundance gradient of ∂[Fe/H]$/\partial Z = -0.34 \pm 0.03$ dex kpc^{-1} from an homogeneous abundance scale for Galactic open clusters, independently of the radial abundance gradient. Indeed, the perpendicular gradient prevails even after correcting the cluster metallicities by the radial abundance gradient. As NGC 2194 is located 0.13 kpc below the Galactic plane, we obtain a [Fe/H] value of -0.04 ± 0.01 from the Z-gradient, if the cluster were placed at the solar Galactocentric distance. The contribution of both radial and pependicular abundance

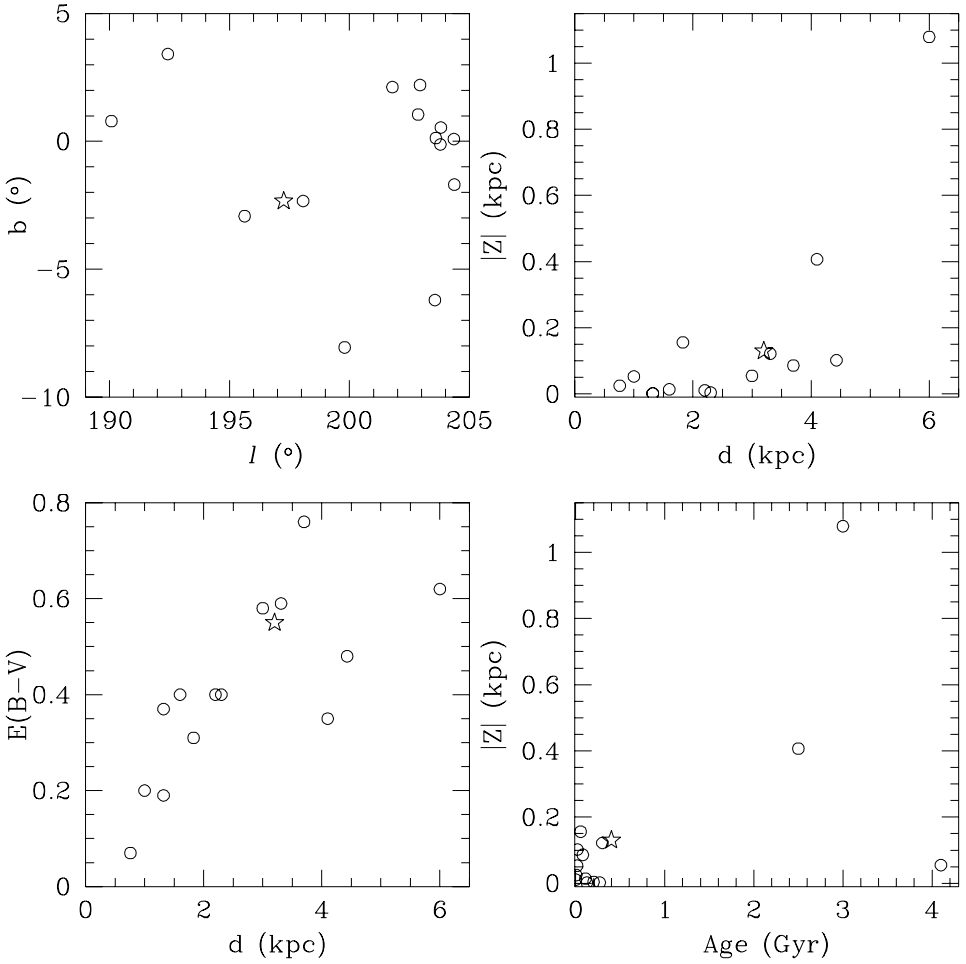

Figure 12. Relationship between the Galactic longitude and latitude, the distance from the Sun, the height out of the Galactic plane, the reddening and the age of open clusters located in the direction towards NGC 2194 (open star) with known fundamental parameters (open circles)(see Section 5 for details).

Table 4. Washington abundance-sensitive indices.

Star	Δ'_1	Δ'_2	Δ'_3	Δ'_4	Δ'_5
248	−0.151	−0.060	−0.201	−0.101	−0.128
672	−0.077	−0.040	−0.107	−0.018	−0.024
1192	−0.135	−0.039	−0.176	–	–
1332	−0.150	−0.013	−0.181	−0.123	−0.127
1379	−0.090	−0.012	−0.103	−0.063	−0.067
1578	−0.154	−0.019	−0.226	−0.108	−0.125
1632	−0.080	+0.002	−0.078	−0.092	−0.069
1698	−0.077	−0.007	−0.111	−0.055	−0.057
2422	−0.116	−0.004	−0.076	−0.098	−0.100

gradients leads to an overall metallicity for NGC 2194 of -0.26 ± 0.02, in excellent agreement with the present cluster metallicity. Hence, NGC 2194 becomes an example of a relatively young open cluster, whose deficiency in metal content is not only due to the fact that it was born far from the Galactic centre in the outer disc, but also that it was born at a relatively high Z value.

6 CONCLUSIONS

We present CCD $VI_{\rm KC}$ photometry for 2515 stars in the field of the open cluster NGC 2194, as well as CCD and photoelectric

Table 5. Fundamental parameters for clusters located in the direction towards NGC 2194.

Cluster	l (°)	b (°)	$E(B-V)$ (mag)	d (kpc)	$\|Z\|$ (kpc)	Age (Myr)	Ref.
NGC 2175	190.08	+00.79	0.40	2.20	0.011	2	1, 2
Bochum 1	192.43	+03.41	0.48	4.43	0.102	20	3, 4
NGC 2169	195.63	−02.92	0.20	1.00	0.053	16	5, 6, 7
NGC 2141	198.07	−02.33	0.35	4.10	0.407	2500	8, 9, 10
Berkeley 22	199.80	−08.05	0.62	6.00	1.079	3000	11
NGC 2259	201.79	+02.12	0.59	3.31	0.122	300	12
Trumpler 5	202.86	+01.05	0.58	3.00	0.055	4100	13
NGC 2264	202.94	+02.20	0.07	0.76	0.025	6	14
NGC 2186	203.56	−06.20	0.31	1.83	0.156	55	4, 15
NGC 2251	203.60	+00.13	0.19	1.32	0.002	270	15
Basel 8	203.79	−00.12	0.37	1.32	0.002	125	15, 16
Basel 7	203.81	+00.54	0.40	1.60	0.014	110	15, 17
NGC 2254	204.35	+00.09	0.40	2.30	0.004	200	15, 18
NGC 2236	204.37	−01.69	0.76	3.70	0.086	80	19

References: (1) Haikala (1995), (2) Grasdalen & Carrasco (1975), (3) Fitzsimmons (1993), (4) Moffat & Vogt (1975), (5) Sagar (1976), (6) Perry, Lee & Barnes (1978), (7) Delgado et al. (1991), (8) Rosvick (1995), (9) Carraro et al. (2001), (10) Burkhead, Burgess & Harsch (1972), (11) Kaluzny (1994), (12) Ann et al. (2002), (13) Kaluzny (1998), (14) Sung, Bessell & Lee (1997), (15) Lyngå (1987), (16) Wagner (1971), (17) Kiral (1969a), (18) Kiral (1969b), (19) Babu (1991).

Washington system photometry of 20 red giant candidates. We have found the following properties for NGC 2194:

(i) The $(V, V - I)$ diagram reveals a broad sequence of stars which traces the cluster MS and a prominent clump of helium burning stars. We show that the broadness of the cluster MS is mainly caused by intrinsic features, such as binarity and/or evolutionary effects, although a small but non-negligible number of field stars located along the line of sight of the cluster are also present.

(ii) A cluster radius of 5.3 arcmin was estimated from star counts in 30-pixel wide rings centred on the cluster. A number of blue straggler star candidates exist, whose overall distribution is localized within 5 arcmin of the cluster centre.

(iii) Through comparison of the cluster $(V, V - I)$ diagram with theoretical isochrones computed by the Padova and Geneva groups, we derived the following values for reddening, distance modulus, age and metallicity: $E(V - I) = 0.75$, $V - M_V = 14.25$, $t = 400$ Myr and $Z = 0.008$.

(iv) A metal abundance $[\mathrm{Fe/H}] = -0.27 \pm 0.03$ relative to the Sun was determined from the Washington system photometry of nine probable red giant members, in good agreement with the value inferred from the isochrones fitting.

(v) NGC 2194 is located at a distance of 3.2 kpc from the Sun and 0.13 kpc below the Galactic plane. The cluster metallicity here derived appears to be compatible with the existence of both a radial and Z-gradient in the Galactic disc. Spectroscopic observations of the red cluster giants will be of great importance and are strongly recommended.

ACKNOWLEDGMENTS

We are gratefully indebted to the CTIO staff for their hospitality and support during the two observing runs. We also thank the referee for his/her suggestions, which have allowed us to improve the manuscript. This work was partially supported by the Argentinian institutions CONICET, SECYT (Universidad Nacional de Córdoba), Agencia Córdoba Ciencia and Agencia Nacional de Promoción Científica y Tecnológica (ANPCyT). This work is based on observations made at Cerro Tololo Inter-American Observatoy, which is operated by AURA, Inc., under cooperative agreement with the NSF.

REFERENCES

Ahumada J., Lapasset E., 1995, A&AS, 109, 375
Alter G., Ruprecht J., Vanisek J., 1979, in Alter G., Bakázs B., Ruprecht J., eds, Catalogue of Star Clusters and Associations. Akademiai Kiado, Budapest
Ann H. B. et al., 2002, AJ, 123, 905
Babu G. S. D., 1991, JA&A, 12, 187
Bessell M. S., 1979, PASP, 91, 589
Burkhead M. S., Burgess R. D., Harsch B. M., 1972, AJ, 77, 661
Burki G., 1975, A&A, 43, 37
Canterna R., 1976, AJ, 81, 228
Canterna R., Harris H. C., 1979, in Philip A. G. D., ed., Problems of Calibration of Multicolour Photometric Systems. Dudley Observatory, Schenectady, NY, p. 199
Carraro G., Chiosi C., 1994, A&A, 288, 751
Carraro G., Hassan S. M., Ortolani S., Vallenari A., 2001, A&A, 372, 879
Clariá J. J., Lapasset E., Bosio M. A., 1990, MNRAS, 249, 193
Clariá J. J., Mermilliod J.-C., Piatti A. E., Minniti D., 1994, A&AS, 107, 39
Clariá J. J., Piatti A. E., Lapasset E., 1998, A&AS, 128, 131
Clariá J. J., Mermilliod J.-C., Piatti A. E., 1999, A&AS, 134, 301
Clariá J. J., Piatti A. E., Lapasset E., Mermilliod J.-C., 2003, A&A, 399, 543
Collinder P., 1931, Medd. Lunds. Astron. Obs. 2
Cousins A. W. J., 1978, Mon. Not. Astron. Soc. S. Afr., 37, 62
Cuffey J., 1943, ApJ, 97, 93
Delgado A. J., Alfaro E., Garcia-Pelayo J. M., Garrido R., 1991, AJ, 103, 891
del Rio G., 1980, A&AS, 42, 189
Fitzsimmons A., 1993, A&AS, 99, 15
Geisler D., 1996, AJ, 111, 480
Geisler D., Clariá J. J., Minniti D., 1991, AJ, 102, 1836 (GCM91)
Geisler D., Piatti A. E., Bica E., Clariá J. J., 2003, MNRAS, in press
Girardi L., Bertelli G., Bressan A., Chiosi C., Groenewegen M. A. T., Marigo P., Salasnich B., Weiss A., 2002, A&A, 391, 195
Grasdalen G. L., Carrasco L., 1975, A&A, 43, 259
Haikala L. K., 1995, A&A, 294, 89
Kaluzny J., 1994, A&AS, 108, 151
Kaluzny J., 1998, A&AS, 133, 25
Kiral A., 1969a, A&A, 3, 327
Kiral A., 1969b, A&A, 2, 25
Landolt A. U., 1992, AJ, 104, 340
Lejeune T., Schaerer D., 2001, A&A, 366, 538 (LS01)
Lyngå G., 1983, Catalog of Open Clusters. Centre de Donnees Stellaires Strasbourg
Mermilliod J.-C., Clariá J. J., Andersen J., Piatti A. E., Mayor M., 2001, A&A, 375, 30
Meynet G., Mermilliod J.-C., Maeder A., 1993, A&AS, 98, 477
Moffat A. F. J., Vogt N., 1975, A&AS, 20, 85
Perry C. L., Lee P. D., Barnes J. V., 1978, PASP, 90, 73
Piatti A. E., Clariá J. J., 2001, A&A, 370, 931
Piatti A. E., Clariá J. J., Abadi M. G., 1995, AJ, 110, 2813
Piatti A. E., Clariá J. J., Bica E., 1998, ApJS, 116, 263
Piatti A. E., Clariá J. J., Bica E., 2000, A&A, 360, 529
Rolleston W. R. J., Smartt S. J., Dufton P. L., Ryans R. S. I., 2000, A&A, 363, 537
Rosvick J. M., 1995, MNRAS, 277, 1379
Ruprecht J., 1966, Bull. Astron. Inst. Czech., 17, 33
Sagar R., 1976, Ap&SS, 40, 447
Sanner J., Altmann M., Brunzendorf J., Geffert M., 2000, A&A, 357, 471
Stetson P. B., 1991, in Worrall D. M., Biemersderfer C., Barne J., eds, ASP Conf. Ser. Vol. 25, Astrophysical Data Analysis Software and Systems I. Astron. Soc. Pac., San Francisco, p. 297
Sung H., Bessell M. S., Lee S.-W., 1997, AJ, 114, 2644
Trumpler R. J., 1930, Lick Obs. Bull. 4, No., 420, 154
Wagner R., 1971, A&A, 14, 283
Wee S. O., Lee M. G., 1996, J. Korean Astron. Soc., 29, S145
Wee S. O., Lee M. G., Geisler D., 1996, J. Korean Astron. Soc., 29, S148

This paper has been typeset from a TEX/LATEX file prepared by the author.